communications earth & environment

ARTICLE

https://doi.org/10.1038/s43247-022-00620-5 OPEN

Present-day warm pool constrains future tropical precipitation

In-Hong Park [1], Sang-Wook Yeh [1✉], Seung-Ki Min [2,3✉], Yoo-Geun Ham[4] & Ben P. Kirtman[5]

Future changes in tropical precipitation affect the livelihood of the world's human population and ecosystems. Climate models project an increased rainfall intensification under anthropogenic warming, but uncertainties in the distribution and magnitude of the changes remain large. Here, we identify a strong positive relationship between the present-day Indo-Pacific warm pool size and projected precipitation changes in the central-to-eastern tropical Pacific using multi-model simulations. Models with larger present-day warm pool size project excessive future warming in the eastern tropical Pacific due to intensified ocean stratification which reduces the zonal sea surface temperature gradient of the tropical Pacific, resulting in the weakening of Walker circulation and precipitation increases in the central-to-eastern tropical Pacific. Based on this relationship, uncertainty in the projected precipitation in the central-to-eastern tropical Pacific can be reduced by approximately 25%, which demonstrates that an improved simulation of present-day Indo-Pacific warm pool size is important for reliable tropical precipitation projections.

[1] Department of Marine Science and Convergence Engineering, Hanyang University, ERICA, Ansan, Republic of Korea. [2] Division of Environmental Science and Engineering, Pohang University of Science and Technology, Pohang, Gyeongbuk, Republic of Korea. [3] Institute for Convergence Research and Education in Advanced Technology, Yonsei University, Incheon, Republic of Korea. [4] Department of Oceanography, Chonnam National University, Gwangju, Republic of Korea. [5] Rosenstiel School for Marine and Atmospheric Science, University of Miami, Miami, FL, USA. ✉email: swyeh@hanyang.ac.kr; skmin@postech.ac.kr

Tropical precipitation is a key component of global climate variability[1,2]. How it responds to increases in greenhouse gas emissions has received much attention because it can significantly influence the hydrological cycle and the global ecosystem[3–5]. Climate models consistently project an increase in tropical precipitation under global warming through a combination of two mechanisms: increased rainfall in wet regions ("wet gets wetter") and increased rainfall in the regions that are expected to experience excessive warming compared to mean surface warming in the tropics ("warmer gets wetter")[6–9]. However, climate-model projections of precipitation in the tropics are less consistent than for the extratropical regions in both sign and magnitude[10,11], which is primarily due to a low signal-to-noise ratio and large degrees of uncertainty[12] (Supplementary Fig. 1). In particular, precipitation in the central-to-eastern tropical Pacific (CETP), defined as the Niño 4 (5°S–5°N, 160°E–150°W) region, which affects western North American drought[13], major monsoons[14], and hurricanes[15] through modulating variabilities of the El Niño Southern Oscillation (ENSO)[16–18], is one of the key regions with the largest uncertainty in future climate projections[12].

A dominant source of uncertainty in future precipitation projections for the CETP can be traced to changes in the zonal structure of Walker circulation[19,20]. While most Climate Model Intercomparison Project phase 5 and phase 6 (CMIP5/CMIP6) models project a weakening of the Walker circulation under global warming[21–24], the robustness of this projection remains unclear because CMIP5/CMIP6 models fail to reproduce observed trends in recent decades and exhibit a large inter-model spread[25].

The Indo-Pacific warm pool (IPWP), where the sea surface temperature (SST) exceeds 28 °C, is associated with variations in atmospheric circulation and deep convection, including Walker circulation[26,27]. As the edge of the IPWP is in contact with the CETP, a strong relationship exists between the variability in the IPWP size and precipitation in the CETP on an inter-annual time scale[28]. Expansion of the IPWP leads to an intensification of the local upward motion by shifting the Walker circulation's asending branch to the east, resulting in increased precipitation in the CETP[27]. However, despite a strong relationship between the IPWP and precipitation in the CETP, climate models often exhibit substantial spreads in mean states and changes in the IPWP size[29,30], enlarging the degree of uncertainty in future precipitation projections for the CETP. Thus, understanding the nature of this inter-model spread in the IPWP is essential to improving the reliability of future precipitation changes in the CETP.

Emergent constraints provide an opportunity to reduce these uncertainties[31–34]. The robustness of the constrained results can be obtained by applying the following three criteria: (1) a plausible mechanism for the emergent relationship, (2) verification of the proposed mechanism, and (3) out-of-sample testing[31]. By analyzing the latest CMIP phase 6 (CMIP6) climate models, we found that a larger IPWP size in the present-day is associated with much weakening of Walker circulation in future climate than a smaller IPWP size, which induces a larger increase in future precipitation amount in the CETP in climate models.

Results

Emergent relationship between future precipitation changes and present-day IPWP size. Historical simulations and shared socioeconomic pathway (SSP) 5–8.5 experiments from 38 CMIP6 models (see Methods and Supplementary Table 1) were used to represent the present-day (1950–1999) and future (2050–2099) climates, respectively[35,36]. Figure 1a depicts future changes in annual mean precipitation and 850 hPa wind in the multi-model ensemble mean (MMEM) of 38 CMIP6 model simulations. All changes were calculated by subtracting the present-day climate from the future climate.

The projected change in tropical precipitation calls for strong increasing trends over the CETP but drying trends in the southeastern Pacific and the eastern Indian Ocean. This pattern is associated with an eastward shift in deep convection and an equatorward shift of the intertropical convergence zone[19,37–39]. The CETP exhibited strong positive trends of precipitation change in future climate with a high inter-model consistency in terms of their sign, while there is a low consistency over the Indian Ocean and western tropical Pacific (Fig. 1a). While strengthening of easterly winds at low levels is dominant over the central Indian Ocean, a weakening of the low-level winds in the eastern tropical Pacific is consistent with the results in CMIP5 climate models[40]. Uncertainty of changes in the low-level winds over the CETP under increased anthropogenic CO_2 is associated with the climatological mean-state bias across the tropical Pacific basin in CMIP6 climate models[41].

Climate models with the largest IPWP sizes in the present-day (solid pink in Fig. 1b) cover most tropical oceans, while climate models with the smallest IPWP sizes in the present-day (solid blue in Fig. 1b and Supplementary Fig. 2) cover the Maritime Continent only. The IPWP size is defined as the ocean proportion enclosed by the 28 °C isotherms in the Indo-Pacific Ocean (30°S–30°N, 40°E–90°W) with a percentage (%) unit. The simulated present-day IPWP size and tropical SST (defined as area-weighted SST mean over 30°S to 30°N, 0 to 360°E) in the 38 CMIP6 climate models exhibit a large inter-model spread and one standard deviations of approximately 10% and 0.5 °C, respectively (Fig. 1c). The large inter-model difference in the IPWP sizes exhibited a strong inter-model relationship with the projected precipitation changes in the CETP: a positive correlation reached up to 0.7 in CMIP6 climate models (Fig. 1d). This implies that the large portion of the uncertainty in future precipitation projection in the CETP is caused by the inter-model differences in the present-day IPWP size simulations.

Influence of the present-day IPWP size on future tropical precipitation changes. Figure 2 illustrates how the inter-model spread of the present-day IPWP size is associated with projected precipitation changes in future climates. Spatial regression of future SST changes onto the present-day IPWP size in CMIP6 climate models shows stronger warming in the CETP than in the western tropical Pacific. This implies that climate models with a large IPWP size in the present-day tend to simulate a large reduction in the future zonal SST gradient of the tropical Pacific than those with a smaller IPWP size (Fig. 2a). Regression patterns of wind changes at 850 hPa exhibit the weakening of trade winds over the tropical Pacific. Weakening of the zonal SST gradient is consistently associated with the strengthening of an ascending motion in CETP and a descending motion in the eastern Indian Ocean and Maritime Continent in future climate scenarios (Fig. 2b).

In addition, climate models with a large IPWP size in the present-day tend to simulate more negative trends of zonal mass stream function over the western Pacific region, where climatologically strong upward motions occur (Fig. 2c). This indicates that the present-day IPWP size is closely tied to the intensity of Walker circulation in future climate, with an eastward shift of its center in the future[21]. Indeed, the zonal position of IPWP's eastern edge in the present-day climate is closely tied to the eastward shift of the Walker circulation's branch in future climate (Supplementary Fig. 3). Similar results were obtained from the CMIP5 climate models (Supplementary Fig. 4).

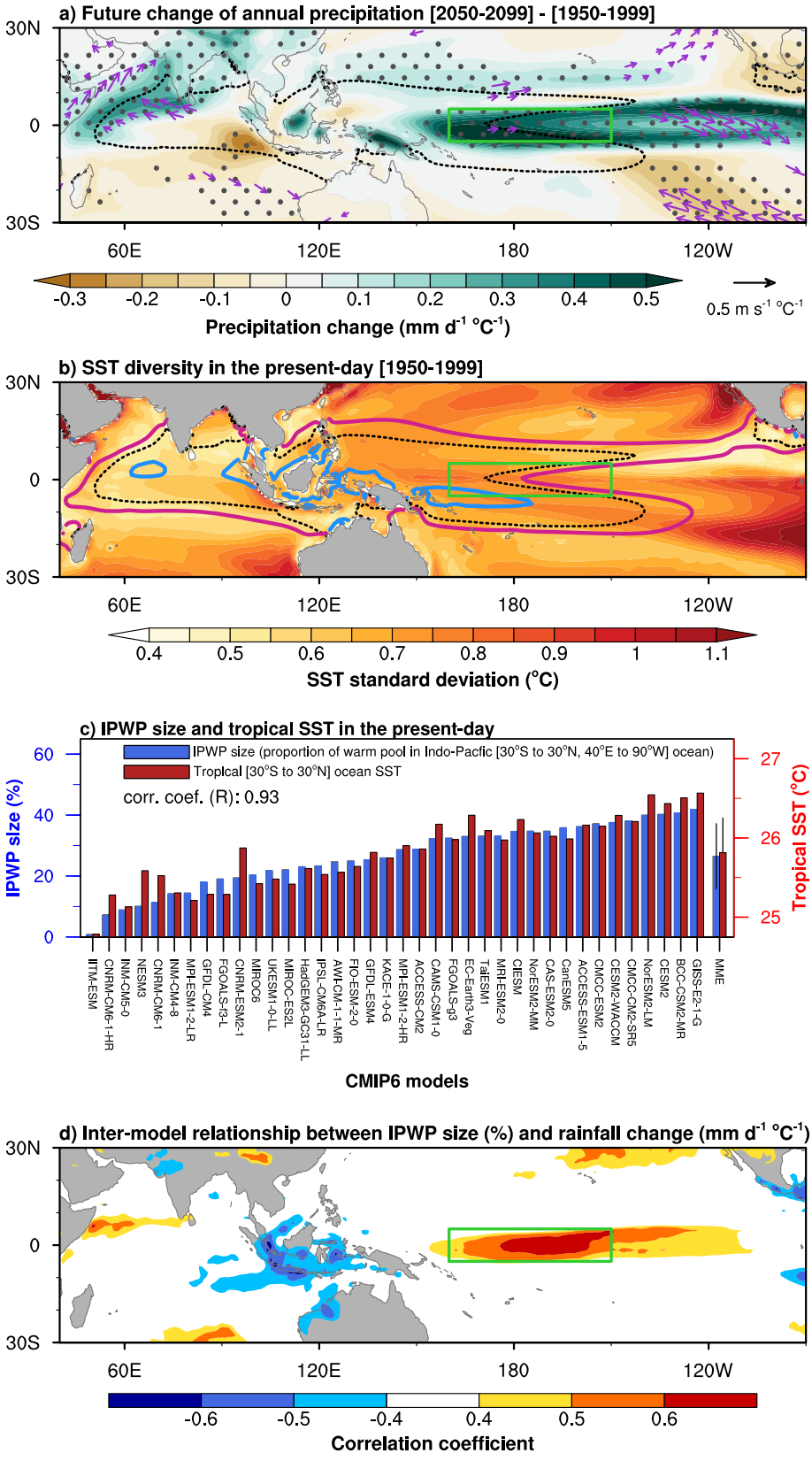

Climate models with a large IPWP size in the present-day tend to simulate a greater reduction in the east-west Pacific SST gradient under global warming compared with those with a small IPWP size in the present-day, resulting in a greater reduction in the zonal gradient of sea level pressure (SLP) over the tropical Pacific (Fig. 3a, b). This is because climate models with a large IPWP size in the present-day (see Fig. 1b) tend to simulate warmer temperatures in the mixed layer of the eastern tropical Pacific compared with those with a small IPWP size (Supplementary Fig. 5a). Climate models with a higher mixed-layer temperature in the eastern tropical Pacific in the present-day tend to simulate a shallow thermocline depth than those with relatively

Fig. 1 Future climate changes, present-day diversity, and the relationship between future tropical precipitation changes and the present-day Indo-Pacific warm pool (IPWP) size. a Multi-model ensemble mean (MMEM) changes of annual precipitation (shading, mm d^{-1} $°C^{-1}$) and 850 hPa wind (vector scale is shown in the bottom right, m s^{-1} $°C^{-1}$) in future climate by 38 CMIP6 models under SSP5-8.5 scenario. Stipples represent the area with a high consistency of the sign in future precipitation changes (>80%, 31 of total 38 models have the same sign). Black dashed lines indicate MMEM of IPWP boundary (28 °C isotherms) in the present-day climate. **b** Inter-model standard deviations of sea surface temperature (SST) (shading) in the present-day. Black dashed lines are the same as in (**a**), and solid pink lines are the averaged IPWP boundary of the five models with the largest IPWP size, while solid blue lines indicate the same for the smallest IPWP boundary of the five models for the present-day. **c** The IPWP size (blue bars) and tropical basin SST (red bars) among climate models in the present-day. Black lines in MMEM illustrate one standard deviation of inter-model values. **d** Inter-model correlations between the projected precipitation changes and the present-day IPWP size among CMIP6 models. In all panels, boxes denote the central-to-eastern tropical Pacific (5°S–5°N, 160°E–150°W, same as Niño 4). Unless otherwise specified, all projected changes are derived from future (2050–2099) minus present-day (1950–1999) values and are normalized by dividing by the global mean surface temperature anomalies of each model.

lower mixed-layer temperatures in the eastern tropical Pacific in the present-day climate (i.e., climate models with a small IPWP size), implying that the upwelling's influence on the surface layer is limited. This feature leads to strong ocean warming in the near-surface layer under greenhouse gas-induced warming, which accelerate ocean stratification under global warming, resulting in the enhanced ocean stratification in the eastern tropical Pacific (Supplementary Fig. 5b). Subsequently, the enhanced ocean stratification in the eastern Pacific is associated with increasing of the dynamical coupling between the ocean and the atmosphere[42], resulting in the weakening of the trade wind and the rapid warming trend of the upper ocean in the eastern Pacific (Supplementary Fig. 5c). This results in reduced east-west zonal SST gradient in climate models with a large IPWP size (Supplementary Fig. 5d), which in turn leads to strong weakening of Walker circulation and enhanced ascending motions with increased precipitation in the CETP in future climate (Fig. 3c, d). The CMIP5 climate models provide similar results to those from the CMIP6 climate models (Supplementary Fig. 6).

Emergent constraint on future precipitation projection in CETP. Large biases related to the IPWP size in the present-day climate could increase uncertainty in projected precipitation in the CETP by modulating the zonal SST gradient in the tropical Pacific. CMIP6 climate models with an excessively large IPWP size in the present-day climate tend to project a larger precipitation increase in the CETP with a statistically significant correlation coefficient ($r = 0.64$, here r is the correlation coefficient) at the 99% confidence level (Fig. 4a). The spread of the simulated IPWP size in the present-day climate explains ~40% of projected precipitation uncertainty in the CETP, based on an "emergent relationship"[31,32,43]. This relationship constrains the probability distribution of the projected precipitation change in the CETP (Methods and Supplementary Fig. 7). After applying the "emergent constraint" between two variables (i.e., present-day IPWP size and future precipitation changes in CETP), projected future precipitation changes in CETP become 0.49 ± 0.17 mm/day (the range of ±1 standard deviation) while unconstraint changes are 0.44 ± 0.23 mm/day. Consequently, a constraint based on the emergent relationship reduces the uncertainty of future precipitation changes by ~25% while overall trends remain similar (Fig. 4b). Emergent constraint based on the tropical mean SST in the present-day exhibits a similar result with 0.47 ± 0.18 mm/day compared to that of the IPWP size. This is due to a close relationship between the IPWP size and tropical mean SST (Fig. 1c). However, the emergent relationship using the present-day tropical mean SST is less strongly linked with the precipitation changes in the CETP in future climate ($r = 0.59$) than that using the IPWP size ($r = 0.64$), resulting in a slight reduction of uncertainty range compared to that of the IPWP size (Supplementary Fig. 8).

We have conducted out-of-sampling tests using a different Earth system model ensemble (CMIP5). Although CMIP5 models are not strictly independent from CMIP6, this out-of-sample testing provides useful evidence of an underlying emergent constraint (Supplementary Fig. 9). Furthermore, the sensitivity test shows that the influence of observational uncertainty and internal climate variabilities on constraints of the CETP precipitation changes is insignificant (Supplementary Fig. 10). To check the influence of outlier models on the emergent relationship obtained from the linear regression analysis, we have also employed the information-theoretic approach to constrain the future CETP precipitation changes (Methods)[44]. This may lead to a reasonable constraint based on the observations by giving more weights on good climate models for simulating the observed IPWP in the present-day. It is found that the main results are similar to those from the linear regression analysis. (Supplementary Fig. 11).

Discussion

We demonstrate that the present-day IPWP size simulated in CMIP6 climate models is closely associated with projected precipitation changes for the CETP, which allows the reduction of uncertainty by the emergent constraint. The large IPWP size in the present-day climate models significantly reduces the east-west Pacific zonal SST gradient in the future climate, resulting in increased precipitation in the CETP due to a strong weakening of Walker circulation (Fig. 5).

Based on the observed IPWP size, the projected uncertainty of the precipitation increase in the CETP is reduced by approximately 25%. Emergent constraints reduce the uncertainty of the precipitation projections in CETP based on a close relationship between future precipitation changes and the present IPWP size biases, but these do not remove all possibility of other model biases. Nevertheless, this can also be applied to estimates of the climate sensitivity with respect to greenhouse gas-induced warming[45], ENSO changes[16], and extreme events[46].

We focused primarily on the atmospheric zonal circulation and convections associated with the simulated IPWP size to explain inter-model variability in projected precipitation anomalies in the CETP. However, it is necessary to examine how other processes, such as surface evaporation, cloud feedbacks, and ocean dynamics influence the relationship between the present-day IPWP size and future precipitation in the CETP. Constrained precipitation projection in the CETP implies that the global atmospheric teleconnections from the tropics would be strengthened[47] in future climate, which has a large potential to increase the occurrence of extreme weather and climate events[16,48]. The present-day IPWP size does not only represent the tropical mean SST (Fig. 1c), but also the change of IPWP size is closely associated with the dynamical variables, including the Walker circulation intensity, zonal SST gradient, and the ocean stratification in the eastern tropical Pacific. Therefore, we are able to provide the physical processes of how the IPWP size can serve as the emergent

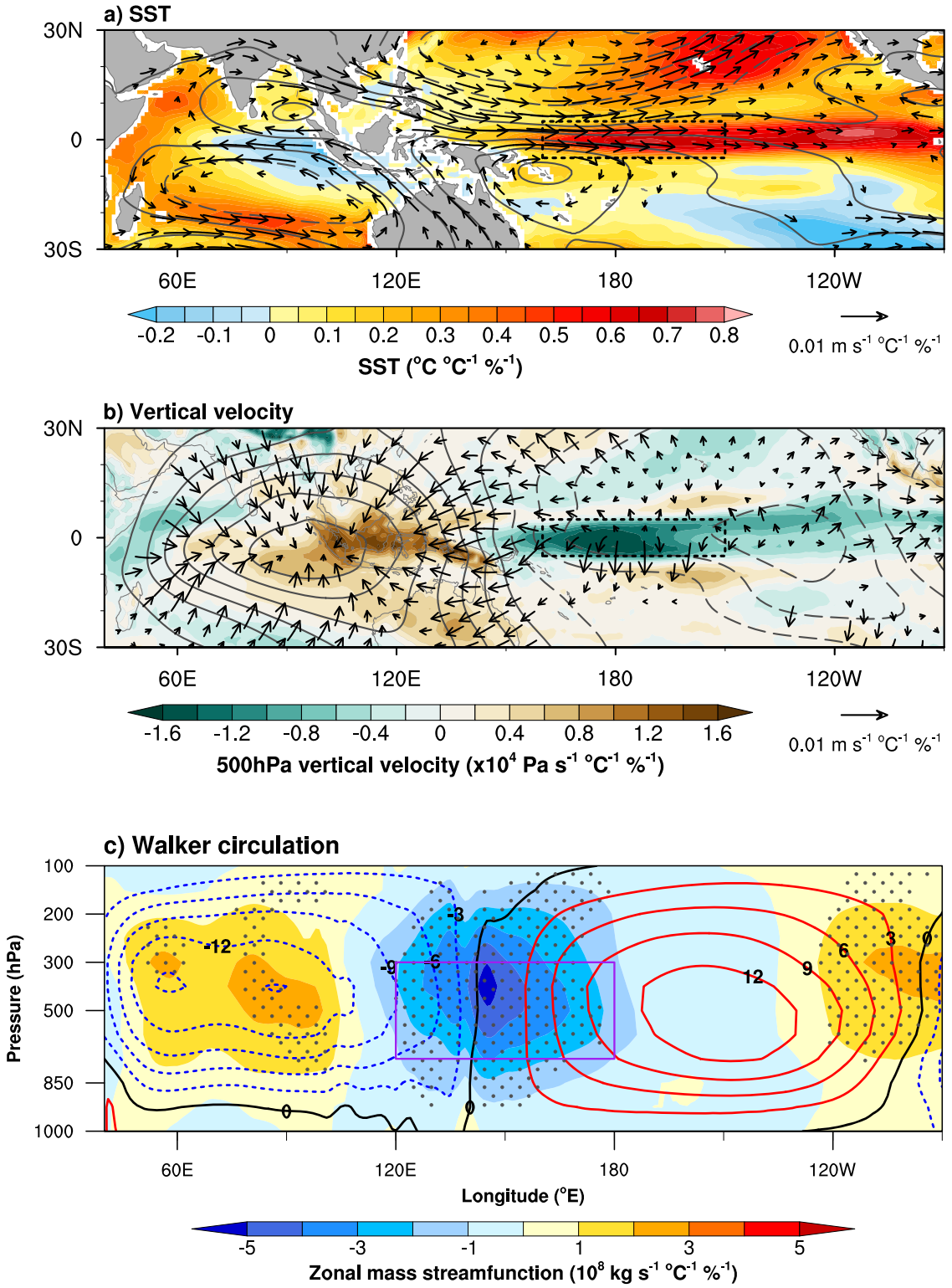

Fig. 2 Inter-model regression patterns of future changes under the SSP5-8.5 scenario onto the present-day IPWP size. a Regressed future changes in SSTs (sea surface temperature, shading: °C), 850 hPa stream function (contour interval: $0.3 \times 10^3\ s^{-1}$), and rotational wind (vectors, $m\ s^{-1}$). **b** Regressed future changes in 500 hPa vertical velocity ($\times 10^4$ Pa s^{-1}; the upward motion is negative), 200 hPa velocity potential (contour interval: $0.3 \times 10^3\ s^{-1}$), and divergent wind (vectors, $m\ s^{-1}$). **c** Regressed future changes in zonal stream function (shading, $10^8\ kg\ s^{-1}$) along the equator (meridional mean between 5°S and 5°N). Contours indicate MMEM of zonal stream function ($10^{10}\ kg\ s^{-1}$) in the present-day (1950–1999). Stipples indicate regions of significance at the 99% confidence level in a student t-test. Positive values indicate a clockwise movement and negative values indicate the reverse; the resulting zero line is the center of the strongest upward motion. The purple box is the region used to define the strength of Walker circulation.

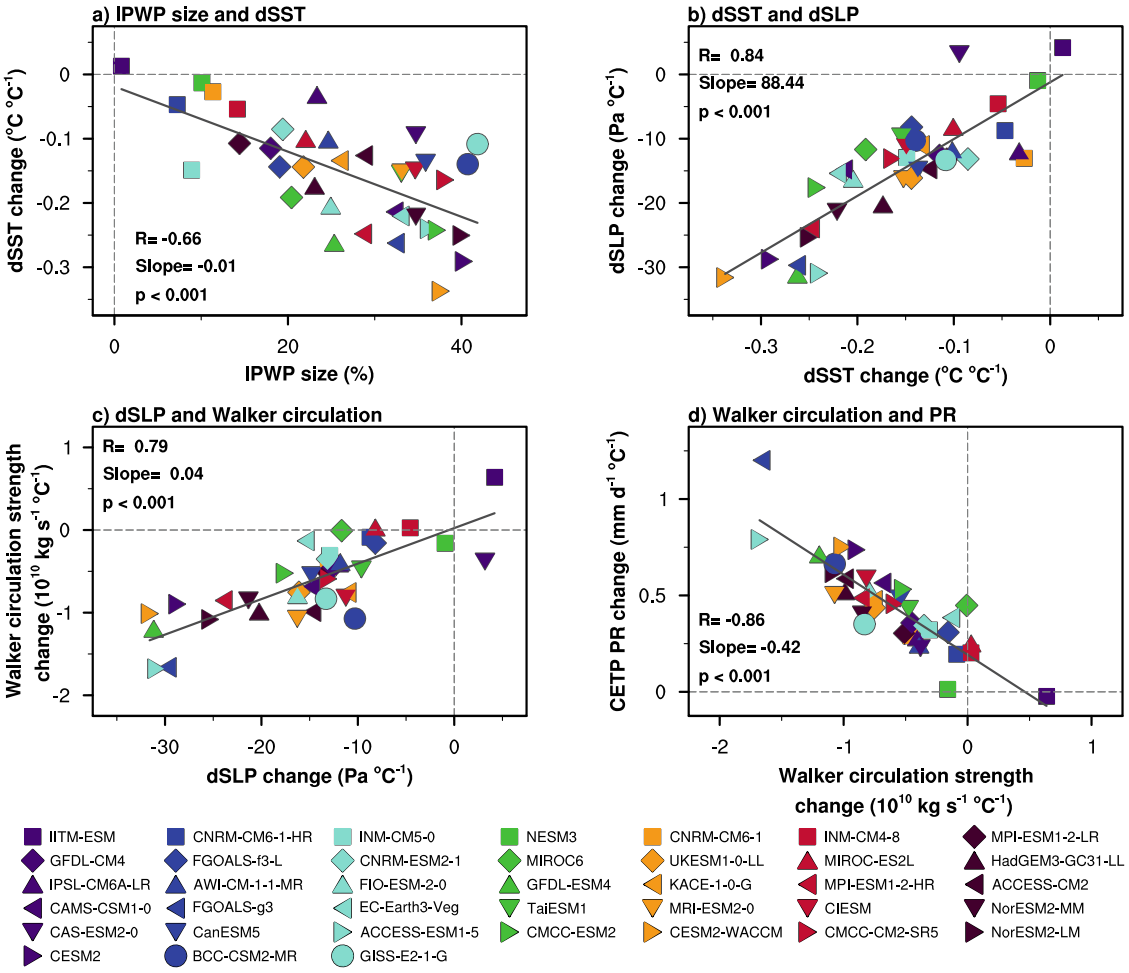

Fig. 3 Inter-model correlation of future projected changes against present-day Indo-Pacific Warm Pool (IPWP) size in SSP5-8.5 scenarios of CMIP6 models. a Simulated present-day IPWP size (%) versus future changes in the Pacific zonal sea surface temperature (SST) gradient (dSST), calculated by east-west, negative values indicate reducing of zonal SST gradient. **b** Future changes in the Pacific zonal SST gradient versus future changes in the Pacific zonal sea level pressure gradient (dSLP). **c** Future changes in the Pacific zonal sea level pressure gradient versus that of Walker circulation strength (10^{10} kg s^{-1}). **d** Future changes of Walker circulation strength (averaging 120°E–180, 700–300 hPa) versus that of CETP (Central-Eastern Tropical Pacific where 5°S–5°N, 160°E–150°W) precipitation (PR, mm day^{-1}). The inter-model correlation coefficients (r), slope, and *p* value displayed in each panel are statistically significant at the 99% confidence level.

constraint of future CETP precipitation changes (Supplementary Figs. 3, 5). Therefore, our result suggests that more realistic simulations of the IPWP size during the present-day climate would be helpful to improve the credibility of simulated projections for climate mitigation and adaptation policy.

Method

Models and observational dataset. We used 38 coupled general circulation models (CGCMs) participating in the CMIP6[35,36]. Details, including model names and modeling groups, are supplied in Supplementary Table 1. Precipitation, SST, SLP, surface air temperature for global mean surface temperature (GMST), vertically integrated water vapor (Q) through the atmospheric column, 500 hPa vertical pressure velocity (ω), ocean potential temperature, and zonal and meridional winds between 1000 and 100 hPa were used, and the criterion for including a given model was the inclusion of whole values for historical and SSP5-8.5 experiments (at the time the data were downloaded until December 2021), except for ocean potential temperature in IITM-ESM and KACE-1-0-G. The upward velocity was negative for ω in this study, unless otherwise specified. We used 1950–1999 mean in historical simulations for the present-day climate, and 2050–2099 mean under SSP5-8.5 as the future climate. Their differences represent future changes under global warming. To validate the CMIP6 results, we use 26 CGCMs from CMIP5 by combining historical (1950–2005) and Representative Concentration Pathway 8.5 (RCP8.5) scenarios for 2006–2099 (Supplementary Table 1).

For observations, we used present-day SSTs from the Hadley Centre Sea Ice and Sea Surface Temperature dataset (HadISST) v1.1[49], Extended Reconstructed Sea Surface Temperature version 5 (ERSSTv5)[50], and Characteristics of Global Sea Surface Temperature Analysis Data (COBE-SST2)[51] for 1950–1999. A common 1° × 1° horizontal grid interpolation was applied to all the model outputs and observations. The present-day climate covers the period from 1950 to 1999 and the future climate refers 2050–2099. To exclude the influence of different climate-response sensitivities to greenhouse gas forcing, all the changes were normalized by dividing them with GMST changes of each model.

Estimating Walker circulation and ocean stratification. We used three indices to estimate Walker circulation from the CMIP5/6 CGCMs. The first index was defined as the difference of the SLP anomaly between the western Pacific (5°S–5°N, 80°E–160°E) and the eastern Pacific (5°S–5°N, 160°W–80°W)[52]. The second index was the same as the first index but for SST[21,24]. The third index was based on a zonal mass stream function[21,53]:

$$\Psi = 2\pi a \int_0^p u_D \frac{dp}{g}$$

where Ψ is the zonal mass stream function, *a* is the radius of the earth, u_D is the divergent component of the zonal wind, *p* is the pressure, and *g* is the gravity constant. The zonal wind was averaged for the meridional band between 5°S–5°N and integrated from the top of atmosphere to surface. In this study, the top level was 100hPa because the stream functions were nearly zero at higher levels. Finally, the strength of Walker circulations was derived from the Ψ average over the Pacific cell region (120°E–180, 700–300 hPa). Ocean stratification was calculated as the difference between the mean temperature over the upper 50 m (representing mixed

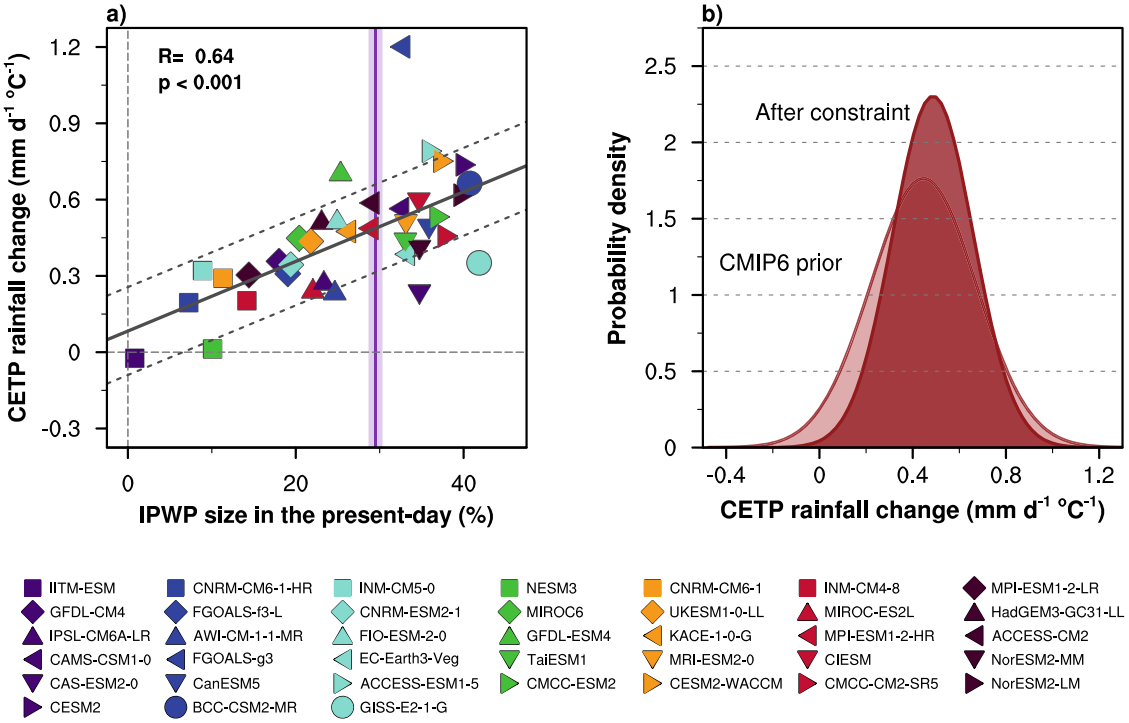

Fig. 4 Emergent constraints on the central-to-eastern tropical Pacific (CETP) precipitation changes in CMIP6. a Projected precipitation changes in the CETP under SSP5-8.5 across the CMIP6 models versus the Indo-Pacific warm pool (IPWP) size in the present-day (1950–1999). The solid gray line follows the linear regression of 38 CMIP6 models, while the dashed gray lines indicate prediction errors with one standard deviation (68% confidence intervals). A solid purple line (shading) indicates the average (one standard deviation) of the observed IPWP size among three datasets: HadISST, ERSSTv5, and COBE-SST2. **b** Probability density functions for the projected precipitation changes in the CETP under SSP5-8.5, before ("CMIP6 prior", transparent) and after ("after constraint", opaque) the emergent constraint is applied.

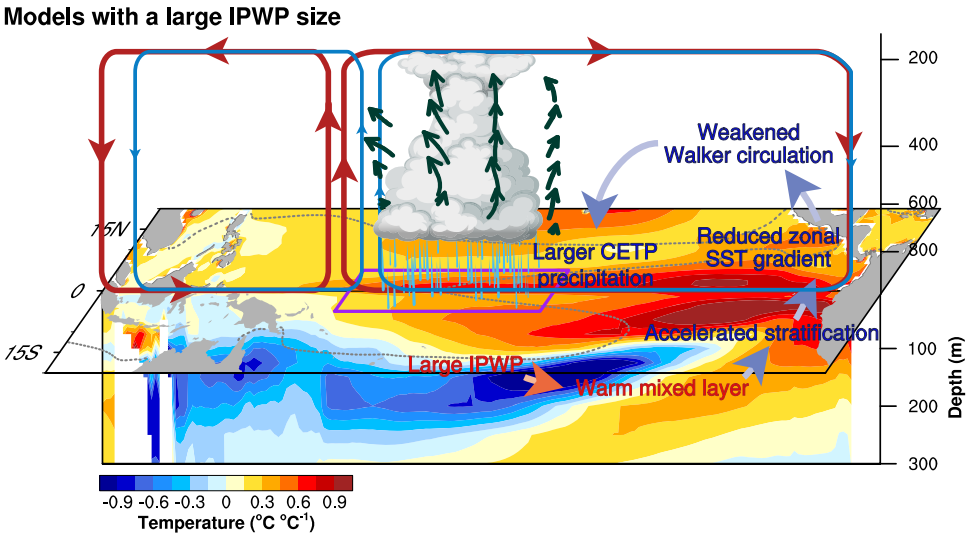

Fig. 5 Schematic diagram showing that the present-day Indo-Pacific Warm Pool (IPWP) constrains future tropical precipitation. Shadings indicate future changes in sea surface temperature (SST) in the Northern Hemisphere and ocean temperature along the equatorial Pacific in the longitude-depth plane (averaged between 5°N–5°S) in climate models with a large IPWP size in the present-day. Vectors illustrate vertical motion. The purple box shows Central-Eastern Tropical Pacific (CETP) region and gray dashed lines represent the IPWP boundary in the present-day. Red text/arrows indicate the present climate, while blue text/arrows indicate changes in the future.

layer) and the temperature at 150 m over the eastern Pacific (5°S–5°N, 160°W–80°W).

Definition of IPWP and CETP precipitation. The IPWP size is that part of the ocean enclosed by the 28 °C isotherms for the Indo-Pacific domain (30°S–30°N, 40°E–90°W) from the annual mean SST. The unit is a percentage, which means the proportion of the IPWP in the entire Indo-Pacific Ocean. The Niño 4 (5°S–5°N, 160°E–150°W) region is defined as the CETP.

Western edge of the Walker circulation and eastern edge of the IPWP. The western edge of the Walker circulation's branch is defined as the zero longitude of Ψ, which is derived from the average from 700hPa to 300hPa over the Indo-Pacific

region (5°S–5°N, 90°E–140°W)[21]. The eastern edge of the IPWP is defined as the longitude crossing 28 °C calculated from the meridional mean of SST in the Pacific (2°S–2°N, 130°E–80°W).

Observational emergent constraint. Probability density functions (PDFs) of the projected precipitation changes in the CETP were calculated following a previously established methodology[54]. The emergent relationship in this study was defined from a linear regression of the CMIP6 models between the simulated present climate state, x_n (IPWP size), and the projected changes y_n (precipitation in the CETP) in the future period (2050–2099). We used an ordinary least squares regression and only one ensemble from each model for equal model weighting. Other regression methods, such as total least squares or averages of multiple realizations based on surface temperature, produced similar results[55,56].

The prior PDF was derived assuming the models were equally likely and following a Gaussian distribution. The PDFs of observational constraints were defined as:

$$P(x) = \frac{1}{\sqrt{2\pi\sigma_x^2}} \exp\left\{-\frac{(x-\bar{x})^2}{2\sigma_x^2}\right\}$$

where $\bar{x}$ is the averaged size of the observed IPWP during the present climate and σ_x is the corresponding standard deviations among three observation datasets.

The "prediction error" of the emergent multi-model linear regression ($\sigma_f(x)$) represents uncertainties around the multi-model linear regression, which produces the probability density of y given x:

$$P\{y|x\} = \frac{1}{\sqrt{2\pi\sigma_f^2}} \exp\left\{-\frac{(y-f(x))^2}{2\sigma_f^2}\right\}$$

where $f(x)$ is the fitted value of the linear regression and σ_f is the prediction error of the linear regression. The emergent relationship was combined with the observational PDF by calculating the product of their PDFs and then integrating across the x-axis variable to derive the constrained PDF:

$$P(y) = \int_{-\infty}^{\infty} P\{y|x\}P(x)dx$$

Information-theoretic approach to constraint. To compare the distribution of the present-day IPWP size between climate model simulations and the observation following a previously established methodology[44], a Gaussian kernel density estimator based on 200 bootstrapped samples makes PDFs with the best bandwidth, which minimizes the mean integrated squared error for normal data. Then, the model weightings are calculated using an information-theoretic distance measure between the PDFs of the observed and modeled IPWP area in the present-day.

$$\Delta_i = \int p(x) log \frac{p(x)}{q_i(x)} dx$$

here, the Kullback–Leibler divergence Δ_i denotes the relative entropy between the observation PDF $p(x)$ and the model PDF $q(x)$ and i indicates each climate model. The smaller the value is, the higher the PDF's agreement between the model and the observation is. Therefore, the exponential of this divergence ($l_i = \exp(-\Delta_i)$) could be used as a weighting of model simulation. To obtain the model weighting (w_i), we use the following normalization:

$$w_i = \frac{l_i}{\sum_i l_i}$$

Future precipitation changes of the CETP are constrained by model weighting from the performance of the present-day IPWP sizes.

Data availability

CMIP5/6 model data were supplied by the Earth System Grid Federation (https://esgf-node.llnl.gov/projects/esgf-llnl/). The observed SST dataset HadISST v1.1 is from the Met Office Hadley Centre (https://www.metoffice.gov.uk/hadobs/). ERSSTv5 and COBE-SST2 data are from NOAA/OAR/ESRL PSD, Boulder, CO, USA (https://www.esrl.noaa.gov/psd/data/gridded/tables/sst.html).

Code availability

All plots and analysis were carried out using NCAR Command Language (NCL) version 6.6.2. All code files are available upon request to boxps@hanyang.ac.kr.

Received: 8 February 2022; Accepted: 9 November 2022;
Published online: 06 December 2022

References

1. Sherwood, S. C., Bony, S. & Dufresne, J.-L. Spread in model climate sensitivity traced to atmospheric convective mixing. *Nature* **505**, 37–42 (2014).
2. Dai, A. Increasing drought under global warming in observations and models. *Nat. Clim. Change* **3**, 52–58 (2013).
3. Messina, J. P. et al. The current and future global distribution and population at risk of dengue. *Nat. Microbiol.* **4**, 1508–1515 (2019).
4. Xie, S.-P. et al. Towards predictive understanding of regional climate change. *Nat. Clim. Change* **5**, 921–930 (2015).
5. Kwiatkowski, L. et al. Emergent constraints on projections of declining primary production in the tropical oceans. *Nat. Clim. Change* **7**, 355–358 (2017).
6. Held, I. M. & Soden, B. J. Robust responses of the hydrological cycle to global warming. *J. Clim.* **19**, 5686–5699 (2006).
7. Chou, C., Neelin, J. D., Chen, C.-A. & Tu, J.-Y. Evaluating the "rich-get-richer" mechanism in tropical precipitation change under global warming. *J. Clim.* **22**, 1982–2005 (2009). J. J. o. C.
8. Schurer, A. P., Ballinger, A. P., Friedman, A. R. & Hegerl, G. C. Human influence strengthens the contrast between tropical wet and dry regions. *Environ. Res. Lett.* **15**, 104026 (2020).
9. Xie, S. P. et al. Global warming pattern formation: sea surface temperature and rainfall. *J. Clim.* **23**, 966–986 (2010).
10. Knutti, R. & Sedláček, J. Robustness and uncertainties in the new CMIP5 climate model projections. *Nat. Clim. Change* **3**, 369–373 (2013).
11. McSweeney, C. F. & Jones, R. G. No consensus on consensus: the challenge of finding a universal approach to measuring and mapping ensemble consistency in GCM projections. *Clim. Change* **119**, 617–629 (2013).
12. Lehner, F. et al. Partitioning climate projection uncertainty with multiple large ensembles and CMIP5/6. *Earth Syst. Dynam.* **11**, 491–508 (2020).
13. Yu, J.-Y. & Zou, Y. The enhanced drying effect of Central-Pacific El Niño on US winter. *Environ. Res. Lett.* **8**, 014019 (2013).
14. Yang, S. et al. El Niño–Southern Oscillation and its impact in the changing climate. *Natl Sci. Rev.* **5**, 840–857 (2018).
15. Kim, H.-M., Webster, P. J. & Curry, J. A. Impact of shifting patterns of Pacific Ocean warming on North Atlantic tropical cyclones. *Science* **325**, 77–80 (2009).
16. Cai, W. J. et al. Increasing frequency of extreme El Nino events due to greenhouse warming. *Nat. Clim. Change* **4**, 111–116 (2014).
17. Kosaka, Y. & Xie, S.-P. Recent global-warming hiatus tied to equatorial Pacific surface cooling. *Nature* **501**, 403–407 (2013).
18. Liu, Y. et al. Recent enhancement of central Pacific El Niño variability relative to last eight centuries. *Nat. Commun.* **8**, 15386 (2017).
19. Kent, C., Chadwick, R. & Rowell, D. P. Understanding uncertainties in future projections of seasonal tropical precipitation. *J. Clim.* **28**, 4390–4413 (2015).
20. Chadwick, R., Boutle, I. & Martin, G. Spatial patterns of precipitation change in CMIP5: why the rich do not get richer in the tropics. *J. Clim.* **26**, 3803–3822 (2013).
21. Bayr, T., Dommenget, D., Martin, T. & Power, S. B. The eastward shift of the Walker Circulation in response to global warming and its relationship to ENSO variability. *Clim. Dynam.* **43**, 2747–2763 (2014).
22. Parsons, L. A. Implications of CMIP6 projected drying trends for 21st century Amazonian drought risk. *Earths Future* **8**, e2020EF001608 (2020).
23. Beobide-Arsuaga, G., Bayr, T., Reintges, A. & Latif, M. Uncertainty of ENSO-amplitude projections in CMIP5 and CMIP6 models. *Clim. Dynam.* **56**, 3875–3888 (2021).
24. Heede, U. K. & Fedorov, A. V. Eastern equatorial Pacific warming delayed by aerosols and thermostat response to CO2 increase. *Nat. Clim. Change* **11**, 696–703 (2021).
25. Plesca, E., Grutzun, V. & Buehler, S. A. How robust is the weakening of the pacific Walker circulation in CMIP5 idealized transient climate simulations. *J. Clim.* **31**, 81–97 (2018).
26. De Deckker, P. The Indo-Pacific Warm Pool: critical to world oceanography and world climate. *Geosci. Lett.* **3**, 20 (2016).
27. Wang, H. & Mehta, V. M. Decadal variability of the Indo-Pacific Warm Pool and its association with atmospheric and oceanic variability in the NCEP-NCAR and SODA reanalyses. *J. Clim.* **21**, 5545–5565 (2008).
28. Chen, N. & Majda, A. J. Simple dynamical models capturing the key features of the Central Pacific El Niño. *Proc. Natl Acad. Sci. USA* **113**, 11732–11737 (2016).
29. Wang, C. Z., Zhang, L. P., Lee, S. K., Wu, L. X. & Mechoso, C. R. A global perspective on CMIP5 climate model biases. *Nat. Clim. Change* **4**, 201–205 (2014).
30. Weller, E. et al. Human-caused Indo-Pacific warm pool expansion. *Sci. Adv.* **2**, e1501719 (2016).
31. Hall, A., Cox, P., Huntingford, C. & Klein, S. Progressing emergent constraints on future climate change. *Nat. Clim. Change* **9**, 269–278 (2019).
32. Thackeray, C. W. & Hall, A. An emergent constraint on future Arctic sea-ice albedo feedback. *Nat. Clim. Change* **9**, 972–978 (2019).

33. Caldwell, P. M. et al. Statistical significance of climate sensitivity predictors obtained by data mining. *Geophys. Res. Lett.* **41**, 1803–1808 (2014).
34. Caldwell, P. M., Zelinka, M. D. & Klein, S. A. Evaluating emergent constraints on equilibrium climate sensitivity. *J. Clim.* **31**, 3921–3942 (2018).
35. Eyring, V. et al. Overview of the coupled model intercomparison project phase 6 (CMIP6) experimental design and organization. *Geosci. Model Dev.* **9**, 1937–1958 (2016).
36. O'Neill, B. C. et al. The Scenario Model Intercomparison Project (ScenarioMIP) for CMIP6. *Geosci. Model Dev.* **9**, 3461–3482 (2016).
37. Huang, P., Zheng, X. T. & Ying, J. Disentangling the changes in the Indian Ocean dipole-related SST and rainfall variability under global warming in CMIP5 models. *J. Clim.* **32**, 3803–3818 (2019).
38. Mamalakis, A. et al. Zonally contrasting shifts of the tropical rain belt in response to climate change. *Nat. Clim. Change* **11**, 143–151 (2021).
39. Sohn, B.-J., Yeh, S.-W., Lee, A. & Lau, W. K. M. Regulation of atmospheric circulation controlling the tropical Pacific precipitation change in response to CO2 increases. *Nat. Commun.* **10**, 1108 (2019).
40. Li, G., Xie, S.-P., He, C. & Chen, Z. Western Pacific emergent constraint lowers projected increase in Indian summer monsoon rainfall. *Nat. Clim. Change* **7**, 708–712 (2017).
41. Seager, R. et al. Strengthening tropical Pacific zonal sea surface temperature gradient consistent with rising greenhouse gases. *Nat. Clim. Change* **9**, 517–522 (2019).
42. Cai, W. et al. Increased variability of eastern Pacific El Niño under greenhouse warming. *Nature* **564**, 201–206 (2018).
43. Ham, Y.-G., Kug, J.-S., Choi, J.-Y., Jin, F.-F. & Watanabe, M. Inverse relationship between present-day tropical precipitation and its sensitivity to greenhouse warming. *Nat. Clim. Change* **8**, 64–69 (2018).
44. Brient, F. & Schneider, T. Constraints on climate sensitivity from space-based measurements of low-cloud reflection. *J. Clim.* **29**, 5821–5835 (2016).
45. Watanabe, M., Dufresne, J.-L., Kosaka, Y., Mauritsen, T. & Tatebe, H. Enhanced warming constrained by past trends in equatorial Pacific sea surface temperature gradient. *Nat. Clim. Change* **11**, 33–37 (2021).
46. Zinke, J. et al. Coral record of southeast Indian Ocean marine heatwaves with intensified Western Pacific temperature gradient. *Nat. Commun.* **6**, 8562 (2015).
47. Barsugli, J. J. & Battisti, D. S. The basic effects of atmosphere–ocean thermal coupling on midlatitude variability. *J. Atmos. Sci.* **55**, 477–493 (1998).
48. Ham, Y. G. & Kug, J. S. ENSO amplitude changes due to greenhouse warming in CMIP5: role of mean tropical precipitation in the twentieth century. *Geophys. Res. Lett.* **43**, 422–430 (2016).
49. Rayner, N. A. et al. Global analyses of sea surface temperature, sea ice, and night marine air temperature since the late nineteenth century. *J. Geophys. Res. Atmos.* **108** (2003).
50. Huang, B. Y. et al. Extended reconstructed sea surface temperature, version 5 (ERSSTv5): upgrades, validations, and intercomparisons. *J. Clim.* **30**, 8179–8205 (2017).
51. Hirahara, S., Ishii, M. & Fukuda, Y. Centennial-scale sea surface temperature analysis and its uncertainty. *J. Clim.* **27**, 57–75 (2014).
52. Vecchi, G. A. & Soden, B. J. Global warming and the weakening of the tropical circulation. *J. Clim.* **20**, 4316–4340 (2007).
53. Yu, B. & Zwiers, F. W. Changes in equatorial atmospheric zonal circulations in recent decades. *Geophys. Res. Lett.* **37**, (2010).
54. Cox, P. M. et al. Sensitivity of tropical carbon to climate change constrained by carbon dioxide variability. *Nature* **494**, 341–344 (2013).
55. Nijsse, F. J. M. M., Cox, P. M. & Williamson, M. S. Emergent constraints on transient climate response (TCR) and equilibrium climate sensitivity (ECS) from historical warming in CMIP5 and CMIP6 models. *Earth Syst Dynam* **11**, 737–750 (2020).
56. Tokarska, K. B. et al. Past warming trend constrains future warming in CMIP6 models. *Sci. Adv.* **6**, (2020).

Acknowledgements

This study was supported by a National Research Foundation of Korea (NRF) grant funded by the Korean government (MSIT) (NRF-2018R1A5A1024958) and the research program for the carbon cycle between ocean, land, and atmosphere of the NRF funded by the MSIT (2021M316A1086803). We acknowledge the World Climate Research Program, which, through its Working Group on Coupled Modeling, coordinated and promoted CMIP5/6. We thank the climate modeling groups for producing and making available their model output, the Earth System Grid Federation (ESGF) for archiving the data and providing access, and the multiple funding agencies who support CMIP5/6 and ESGF.

Author contributions

I.-H.P. and S.-W.Y. contributed equally to designing the research. I.-H.P. performed the data analysis and, together with S.-W.Y., interpreted the results. I.-H.P. wrote the manuscript and edited it together with S.-W.Y. All of the authors (I.-H.P., S.-W.Y., S.-K.M., Y.-G.H., and B.P.K.) discussed the study results and reviewed the manuscript.

Competing interests

The authors declare no competing interests.

Additional information

Supplementary information The online version contains supplementary material available at https://doi.org/10.1038/s43247-022-00620-5.

Correspondence and requests for materials should be addressed to Sang-Wook Yeh or Seung-Ki Min.

Peer review information *Communications Earth & Environment* thanks the anonymous reviewers for their contribution to the peer review of this work. Primary Handling Editors: Clara Orbe, Joe Aslin, Heike Langenberg and Aliénor Lavergne. Peer reviewer reports are available.

Reprints and permission information is available at http://www.nature.com/reprints

Publisher's note Springer Nature remains neutral with regard to jurisdictional claims in published maps and institutional affiliations.